Journal of Molecular Structure 1238 (2021) 130464

Contents lists available at ScienceDirect

Journal of Molecular Structure

journal homepage: www.elsevier.com/locate/molstr

Dye sensitized solar cell-based optoelectronic device using novel [Ru(L1)(L2)(NCS)$_2$] complex

Osman Dayan[a], Arife Gencer Imer[b,*], Melek Tercan[a], Aysegul Dere[c], Abdullah G. Al-Sehemi[d,e,f], Ahmed A. Al-Ghamdi[g], Fahrettin Yakuphanoglu[c,g]

[a] Çanakkale Onsekiz Mart University, Faculty of Science and Arts, Department of Chemistry, 17100, Çanakkale, Turkey
[b] Department of Physics, Faculty of Science, Van Yuzuncu Yil University, 65080, Van, Turkey
[c] Nanoscience and Nanotechnology Laboratory, Firat University, Elazig, Turkey
[d] Department of Chemistry, Faculty of Science, King Khalid University, Abha 61413, P.O. Box 9004, Saudi Arabia
[e] Research Center for Advanced Materials Science, King Khalid University, Abha 61413, P.O. Box 9004, Saudi Arabia
[f] Unit of Science and Technology, Faculty of Science, King Khalid University, Abha 61413, P.O. Box 9004, Saudi Arabia
[g] Department of Physics, Faculty of Science, King Abdulaziz University, Jeddah 21589, Saudi Arabia

ARTICLE INFO

Article history:
Received 20 January 2021
Revised 4 April 2021
Accepted 6 April 2021
Available online 13 April 2021

Keywords:
Ru complex
Photosensor
Photoresponse
Illumination effect

ABSTRACT

A dye sensitized solar cell-based photodiode was prepared using novel [Ru(L1)(L2)(NCS)2] complex for solar energy and optoelectronic applications. The new heteroleptic ruthenium(II) complex [Ru(L1)(L2)(NCS)$_2$], was synthesized from the reaction of (pyridyl)benzimidazole ligands. The possible usage of [Ru(L1)(L2)(NCS)$_2$] complex in dye synthesized solar cell-based photodiode was investigated using electrical and capacitance characteristics. The device was irradiated under various solar light intensities. The change in photocurrent of the device confirms the photoconducting behavior of prepared device. The device exhibited both the photocapacitance and photoresponse behavior with solar illumination. The obtained optoelectrical results suggest that the studied photodiode with [Ru(L1)(L2)(NCS)$_2$] complex could be used in optoelectronic device for optical switching and controlling applications.

© 2021 Elsevier B.V. All rights reserved.

1. Introduction

Metal complexes have been considerably interested in optoelectronic technology especially for optical controlling devices such as photodiode, photodetector and optical sensor [1–4]. As the molecules absorb light, the light energy is converted into a molecular chemical energy and this energy is stored in an excited state for a short–time, thus molecular photodiodes are formed which are prone to charge transfer reactions [1]. Benzimidazole and pyridine derivative ligands are strong basic ligands due to an aromatic nitrogen group [2], and their Ru complexes possess superior photochemical and photophysical properties [3]. Such complexes are unique for applications such as photocatalysis, photochemistry and electrochemistry [4]. In Ru–polypyridine type complexes, it is possible to raise the light absorption by modifications on the ligands [5] and to prepare complexes having high oxidation potentials hence having different band gaps [6]. Due to the ease of use, availability and cheapness of metal complexes, their optical, photonic and electronic properties have been investigated [3–10]. The light absorption properties of Ru – polypyridine type complexes suggest that they can be used as photoconductive materials. Because of these properties, a new type of photodiode was fabricated in the present study. Although there are many reports on the synthesis of Ru complexes [3–11], to the best of our knowledge there is no study about the synthesis of [Ru(L1)(L2)(NCS)2] $_{complex.}$ Thus, in present study, firstly, 2–(6–methylpyridine–2–yl)–1–(3,4,5–trifluorobenzyl)–1*H*–benzimidazole ligand **(L1)** was coordinated to [RuCl$_2$(p–cymene)]$_2$, then [Ru(L1)(L2)(NCS)$_2$] complex was synthesized by using 6–(1*H*–benzimidazol–2–yl)pyridine–2–carboxylic acid ligand **(L2)** and NH_4(NCS), and the photochemical properties of [Ru(L1)(L2)(NCS)$_2$] complex was characterized by H, C-NMR, SEM- EDX, MS, UV–Vis and FT-IR methods. Secondly, the synthesized complex was used in optoelectronic device fabrication as dye synthesized solar cell-based photodiode for the first time. The photoresponse and photocapacitance properties of the device were analyzed in detail using current-voltage (I-V), and transient measurements. The obtained results were analyzed via impedance-voltage techniques in a wide range of frequencies to understand the photocapacitance and photoconductance behavior of fabricated device.

* Corresponding author at: Department of Physics, Van Y.Y.U, Van, Turkey.
E-mail address: agencerimer@yyu.edu.tr (A. Gencer Imer).

https://doi.org/10.1016/j.molstruc.2021.130464
0022-2860/© 2021 Elsevier B.V. All rights reserved.

2. Experimental details

2.1. Materials & methods

The solvents and the chemicals were purchased and used without purification. UV–Vis spectra were taken by Perkin–Elmer Lambda 35 UV in the range of 200–900 nm, and Perkin–Elmer Spectrum One FTIR system was used for infrared measurements. ^{1}H–NMR and ^{13}C–NMR spectra were acquired on JEOL NMR–400 MHz. Mass spectrum of [Ru(L1)(L2)$(NCS)_2$] complex was recorded by Shimadzu LC–MSMS–8040 mass spectrometer. JEOL SEM–7100–EDX system was used to analyze the chemical composition of the complex. Cyclic voltammetry was carried out with a BST8–stat EIS analyzer (ENTEK Electronics). Schimadzu RF–5301 PC spectrofluorophotometer was used to monitor the photoluminescence spectra.

2.2. Synthesis of [Ru(L1)(L2)$(NCS)_2$] complex

2.2.1. Synthesis of ***L1*** ligand

2–(6–methylpyridin–2–yl)–1*H*–benzimidazole (prepared according to the relevant literature [16]) (400 mg, 1.91 mmol) was dissolved in acetone (20 mL), then KOH (118 mg, 2.10 mmol) added to the reaction media and refluxed for 8 hours. After cooling to room temperature, 3,4,5–trifluorobenzyl chloride (345 mg, 1.91 mmol) in acetone was added and stirred for a few hours first, then refluxed for 8 hours. Finally, acetone was removed and the resulting beige colored solid was washed with water, crystallized from ethanol. (Yield: 76 %)

FTIR (υ, cm^{-1}): 3029, 2989, 2934, 1619, 1578, 1528, 1467, 1445, 1426, 1395, 1351, 1328, 1041, 993, 845, 801, 785, 736, 705, 673, 595, 570, 507, 440.

^{1}H–NMR (400 MHz, $CDCl_3$) δ ppm 2.49 (s, 3 H) 6.05 (s, 2 H) 6.85 (t, j= 7.25 Hz, 2 H) 7.18 (d, j=7.70 Hz, 1 H) 7.29 (m, 2 H) 7.72 (t, j=7.81 Hz, 1 H) 7.85 (d, j= 8.23 Hz, 1 H) 8.24 (d, j= 7.89 Hz, 1 H).

^{13}C–NMR (100 MHz, $CDCl_3$) δ ppm 24.39; 48.17; 109.77; 110.20; 111.19; 120.57; 121.87; 123.03; 123.46; 123.74; 123.98; 134.21; 136.56; 137.40; 142.76; 149.36; 149.80; 150.13; 152.53; 157.52.

2.2.2. Synthesis of ***L2*** ligand

L2 ligand was synthesized according to the related literature [12].

2.2.3. Synthesis of [Ru(L1)(L2)$(NCS)_2$] complex

L1 (115 mg, 0.327 mmol) and [$RuCl_2$(*p*–cymene)]$_2$(100 mg, 0.163 mmol) were dissolved in dichloromethane and mixed for 8 hours under room temperature. After complex formation, dichloromethane was removed and the remaining complex was dissolved with dimethylformamide (DMF). L2 ligand (68 mg, 0.327 mmol) was added to the reaction mixture at the boiling temperature and refluxed overnight. The reaction was cooled to room temperature, ammonium thiocyanate (124 mg, 1.63 mmol) was added and refluxed for a few hours. Then DMF was distilled under vacuum and the complex was purified by washing with water followed by ethanol and diethyl ether. (Yield: 55 %).

FTIR (υ, cm^{-1}): 3060, 2989, 2930, 2105, 1966, 1715, 1620, 1594, 1531, 1478, 1448, 1406, 1355, 1235, 1153, 1046, 806, 787, 747.

^{1}H–NMR (400 MHz, DMSO–d_6) δ ppm 2.97 (s, 3 H) 6.12 (s, 2 H)7.21 (t, j= 7.21 Hz, 2 H) 7.33–7.39 (m, 3 H) 7.43 (d,j= 7.69 Hz, 1 H) 7.66–7.81 (m, 5 H) 7.93 (t, j= 7.79 Hz, 2 H) 8.16 (d, j= 7.81 Hz, 2 H).

LC–MS/MS (CH_3CN) m/z: found (calc.) $[M]^+$, 809 (808.8); $[M - NCS^-]^+$, 751 (751), $[M–CH_2–C_6H_2F_3]^+$, 664 (664.7).

2.3. Preparation of the dye sensitized solar cell-based photosensor

The dye sensitized solar cell-based photosensor using synthesized [Ru(L1)(L2)$(NCS)_2$] complex was prepared using FYTRONIX solar cell kit containing the titanium oxide photoanode, platinum cathode and iodolyte AN-50. The active area of studied device is 0.36 cm^2. The electrical characteristic of studied device was performed by FYTRONIX FY-9000 electronic device characterization system (Fig. 1a) at room temperature. The transient photoconductance, photocapacitance and photocurrent analysis of device were automatically recorded using FYTRONIX 9000 full automatic solar simulator in the power range of 20–100 mW/cm^2 with AM 1.5 filter and a spectral matching.

3. Results and discussion

3.1. Structural characterization of the complex

In this work, we have synthesized a new heteroleptic Ru(II) complexes bearing (pyridyl)benzimidazole ligands. The synthesis of [Ru(L1)(L2)$(NCS)_2$] complex is depicted in Scheme 1. The complex was characterized by NMR, MS, FT–IR, UV–Vis and Fluorescence spectroscopies. The surface morphology and elemental distribution

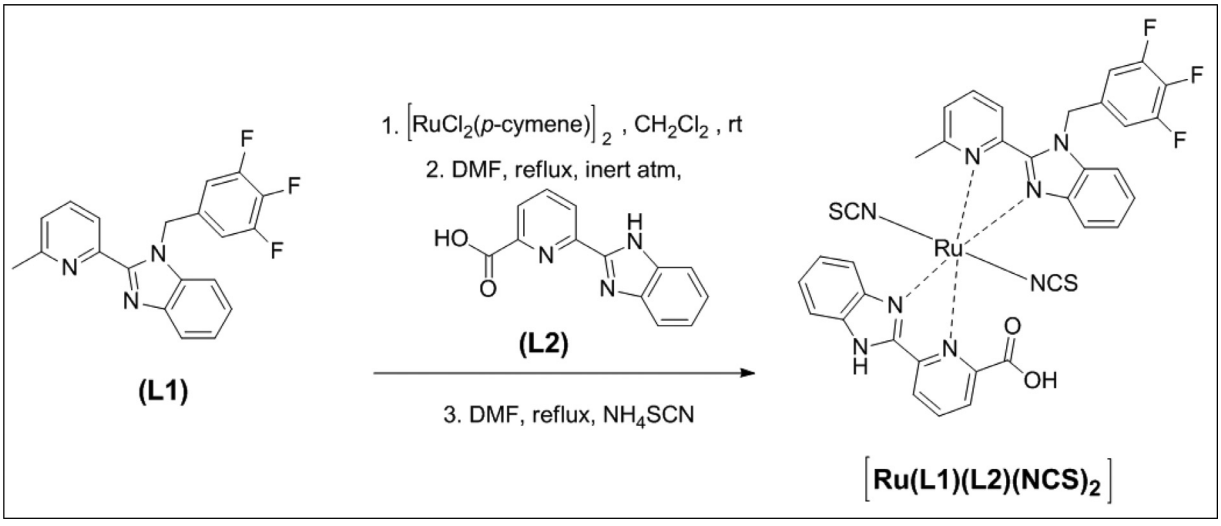

Scheme 1. Synthesis of [Ru(L1)(L2)$(NCS)_2$] complex.

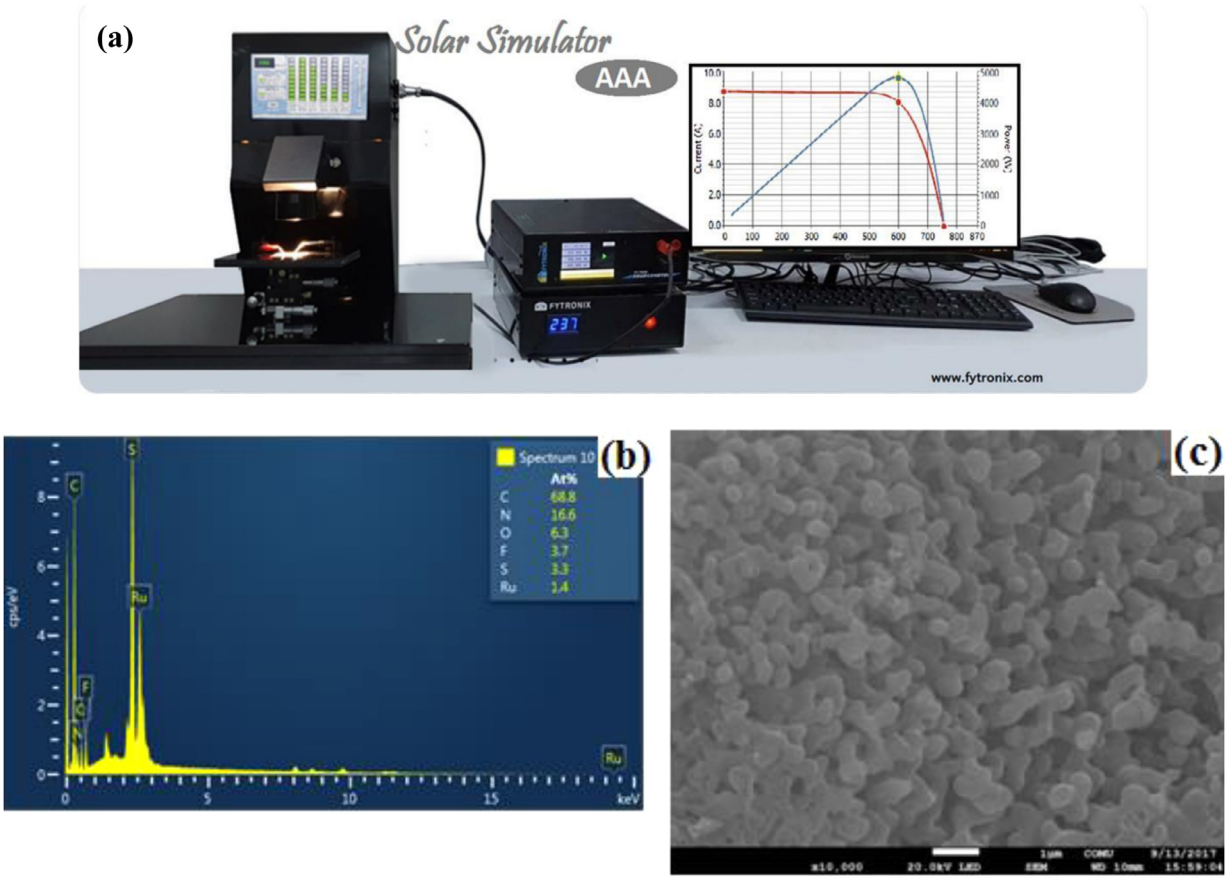

Fig. 1. a FYTRONIX 9000 full automatic solar simulator system
b) EDX spectrum c) SEM image of $Ru(L1)(L2)(NH_4NCS)_2$ complex (Ru: 1.4 %).

of complex were performed by SEM–EDX technique. Additionally, the electrochemical property of the complex was investigated with cyclic voltammetry.

There is a good agreement between the calculated mass of $[Ru(L1)(L2)(NCS)_2]$ complex and its LC–MS/MS spectra. The molecular ion peak at m/z = 664 corresponds to the mass loss of $–CH_2–C_6H_2F_3$ fragment. The other stable peak at m/z = 751, demonstrates the fragmentation of –NCS ligand. From the ^{1}H–NMR spectra, $–CH_3$ and $–CH_2–$ protons of **L1** were observed at 2.49 and 6.05 ppm as singlet, respectively. After the complexation, these protons were shifted at 2.97 and 6.12 ppm as singlet, respectively. In the FT–IR spectra of complex, the NCS^- ligand gave strong band at 2105 cm^{-1}. EDX spectrum and SEM image of the complex are shown in Fig. 1(b-c). As seen in Fig. 1b, C, N, O, F, S, Ru elements are observed in EDX spectra of the complex. The presence of these elements in EDX confirms the chemical composition of the complex. Also, as seen in SEM image (Fig. 1c), the complex is formed the particles. The distribution of the particles is almost homogenous on the complex. The particles do not have a regular shape and their sizes differ. The particles appear as a single particle in the structure and connect someone. The space between particles increases the light absorption, when the complex is irradiated with sun light. The increase in light absorption of the complex improves the photoconductive properties of the material.

3.2. Optical properties of $[Ru(L1)(L2)(NCS)_2]$ complex

The UV–Vis absorption and emission spectrum of $[Ru(L1)(L2)(NCS)_2]$ complex, recorded in DMSO, were analysed and a small shift to red wavelength was observed at around 500 nm compared to **L1** ligand. Also very slight absorption around 500 nm refers the MLCT transition (Fig. 2).

Table 1
Optical and electrochemical data for $[Ru(L1)(L2)(NCS)_2]$ complex.

Absorption, λ_{max} (nm)	E_{ox}, (V/NHE)	E_{red}, (V/NHE)	$E_{band-gap}$,[a] (eV)
318-. 510 (d–Π*)	1.57	–0.73	2.30

[a] UV–Vis absorption spectrum was monitored in DMSO for 1 × 10^{-5} M $[Ru(L1)(L2)(NCS)_2]$ complex.

3.3. Electrochemical properties of $[Ru(L1)(L2)(NCS)_2]$ complex

Cyclic voltammogram of $[Ru(L1)(L2)(NCS)_2]$ complex was examined with 0.1 M $LiClO_4$ in DMF (Fig. 3). The oxidation potentials of the Ru complex (vs. Fc/Fc^+ ferrocene redox couple) at the excited state and the ground state were calculated by using the related equations (a and b) and the oxidation potential of $[Ru(L1)(L2)(NCS)_2]$ complex was found 0.93 V. The data were given in Table 1 by converting NHE. Also the energy level diagrams of the complex, semiconductor and the electrolyte are represented in Fig. 4.

Cyclic voltammogram of the complex was recorded in 0.1 M $LiClO_4$ in DMF (as a supporting electrolyte). By adding 0.64 V, oxidation potential of $[Ru(L1)(L2)(NCS)_2]$ complex was converted to NHE (equation a: $E_{HOMO} = E_{ox} + 0.64$). The oxidation potential of excited state and ground state, E_{ox} and E_{red} were calculated by following equations: equation b: $E_{LUMO} = E_{HOMO} - E_{band-gap}$, equation c: $E_{band-gap} = 1241(eV)/\lambda_{max(onset)}$

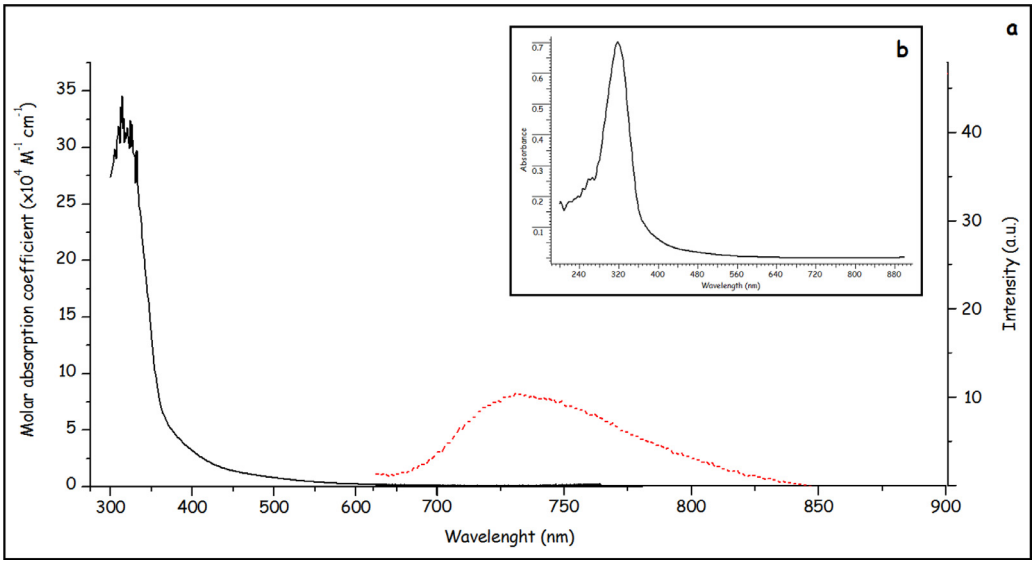

Fig. 2. **a**: Overlapped UV–Vis and emission spectrum of [Ru(L1)(L2)(NCS)$_2$] complex (1×10^{-5} M in DMSO, λ_{exc}: 550 nm, slit: 15 nm) b: UV–Vis spectrum of L1 ligand.

The calculated energy band gap for [Ru(L1)(L2)(NCS)$_2$] complex is 2.30 V. For a less energy favoured electron transfer, LUMO energy level of the complex must be lower than the electrolyte and HOMO energy level of the complex must be above the conductivity band of TiO_2. As given in Fig. 4. [Ru(L1)(L2)(NCS)$_2$] complex has a proper energy band gap which allows the electron transfer.

3.4. Photocurrent-voltage characteristics of the photodiode based on [Ru(L1)(L2)(NCS)$_2$] complex

It is crucially important to understand the photoelectrical characteristic of the dye-sensitized solar cell-based photodiode under various illumination intensities for its using in an optoelectronic device fabrication. It is seen in Fig. 5 that the device exhibit an exponential behavior of dark current (I_{dark}) with applied voltage at the dark condition. Fig. 5 also shows the current-voltage properties of the photodiode under the illumination. As seen in Fig. 5 figure that the reverse current increases when the illumination intensity increases, while the current does not change at the forward biasing with the increasing in the light power. This means that the number of photogenerated carriers enhances with the illumination power due to the dissociation of the neutral Frenkel excitons, so that the photocurrent (I_{ph}) is created by absorption of the energy of the incident photon [7]. Thus, the device has highly good photosense property, and typically exhibits the photoconductive behavior for an ideal photodiode [13]. The photosensitivity (S) of the photodiode is defined by the following relation [13–15]

$$S = \left[(I_{ph} - I_{dark})\right]/I_{dark} \quad (1)$$

Table 2 presents the calculated S values of dye sensitized solar cell device under different solar light intensities. As seen in Table 2, its light sensitivity clearly enhances when the illumination power increases, and reached to the value of 11,536.13 for 100 mW/cm^2 at -3 V; this value is almost 16 times greater than the device reported in ref. [16]. Also this studied device has the higher photosensitivity that of 1703.04 for the Au/indigo carmine/n-Si/Al photodiode [14].

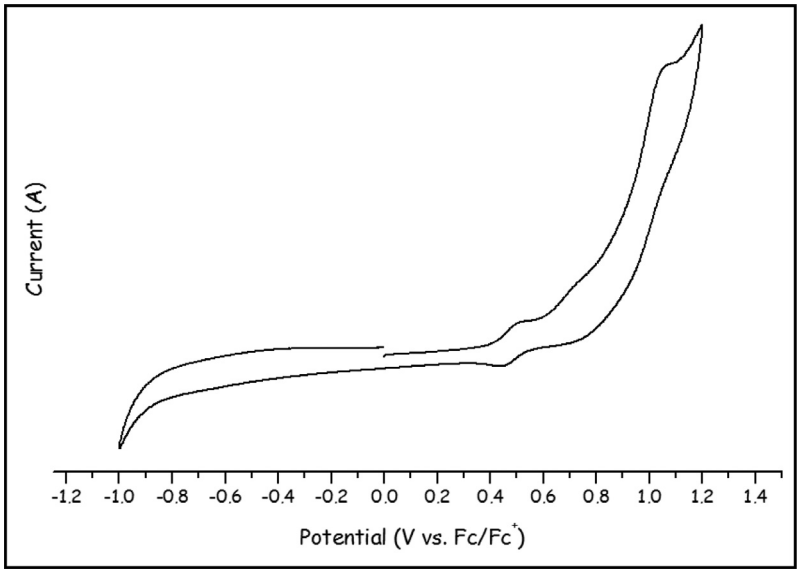

Fig. 3. Cyclic voltammogram of [Ru(L1)(L2)(NCS)$_2$] complex (0.1 M $LiClO_4$ (in DMF) was used as a supporting electrolyte and the data was examined at 50 mV/s, Fc/Fc$^+$couple was used as an external standard.).

Table 2
Photosensitivity and photoresponse ratio of the dye synthesized solar cell-based photodiode under various illumination conditions.

Power	I_{sc}	V_{oc}	I_{ph} (at -3 V)	Photosensitivity, S			Photoresponse ratio, R_{ph}		
(mW/cm^2)	(A)	(V)	(A)	-1 V	-2 V	-3 V	-1 V	-2 V	-3 V
20	1.38×10^{-5}	0.12	1.70×10^{-5}	2814.78	2075.69	2075.69	29.15	21.76	17.21
40	3.06×10^{-5}	0.12	3.70×10^{-5}	6603.38	4872.21	3833.13	67.03	49.72	39.33
60	4.65×10^{-5}	0.12	6.18×10^{-5}	10,631.65	7933.52	6145.40	107.32	80.34	62.45
80	6.33×10^{-5}	0.12	8.92×10^{-5}	15,419.21	11,422.26	8920.22	155.19	115.22	90.20
100	7.71×10^{-5}	0.09	1.15×10^{-4}	19,968.94	14,785.03	11,536.13	200.69	148.85	116.36

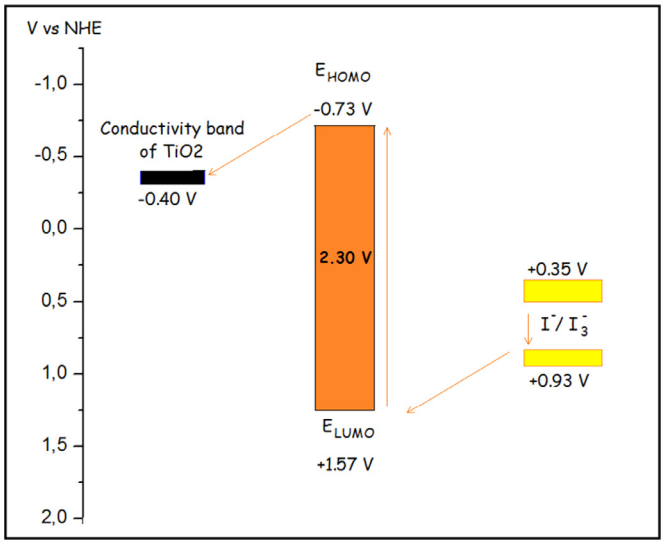

Fig. 4. Energy level diagram for [Ru(L1)(L2)(NCS)$_2$] complex.

This increment in the photosensitivity could be attributed to the photogenerated charges by the applied electric field [15].

Considering the efficiencies of the Ru complexes as dye sensitized solar cells (DSSC), the photovoltaic parameters of DSSC based on [Ru(L1)(L2)(NCS)$_2$] complex were investigated and compiled in Table 2 under various illuminations. Although the energy band gap of the complex was featured to allow the e–transfer, significant photovoltaic activity could not be observed (η%= 0.03 under 100 mW/ cm^2) for the studied device. This high photosensitivity values suggests that the device is good enough to work as a photodiode.

Another important parameter is the photoresponsivity (R) to investigate the characteristics of the photodiode. The photoresponsivity (R) of the photodiode can be defined by the following equation [15]

$$R = I_{ph}/P.A \quad (2)$$

where P is the solar light power, A is the area exposed to the incident light. Fig. 6 presents the photoresponsivity-voltage plots of the dye sensitized solar cell-based photodiode at reverse biasing under various light intensities. As seen from this figure that the photoresponsivity exponentially increases with an applied voltage (at reverse biasing) under the all photo illumination intensities. These results confirm that the fabricated dye sensitized solar cell-based photodiode can be used in the fabrication of organo-optoelectronic devices such as photosensor [13–17].

For further determining of the photosensing behavior of the photodiode, the relation between the photocurrent density and solar light power is defined as [17,18];

$$J_{Ph} = CL^m \quad (3)$$

where the exponent m is important to understand photocurrent mechanism, calculated by the tangent of the fitted line in Fig. 7. From this figure, the photocurrent shows an excellent linearity with the photo illumination power, and the value of m for the dye sensitized solar cell-based photodiode was found to be 1.18, which suggests the photocurrent mechanism controlled by the recombination centers of the studied photodiode [16], and also the photosensing behavior of the device was analyzed using FYTRONIX solar simulator I V characterization system. The system suggests that the photoresponse mechanism of the diode is controlled by the recombination centers.

One of the significant properties is the linear dynamic change range (LDR) to characterize photodiodes. The plotted line shown in Fig. 7 was used to understand the LDR behavior of dye sensitized solar cell-based photodiode. The LDR value of studied device was determined as 26.82 dB in the range of 20–100 mW/cm^2, and this LDR value is smaller than that of 60 dB for Al/p-Si/B-doped GO/Au photodiode [18].

3.3. Transient photocurrent, photocapacitance and photoconductance characteristics of the photodiode

The photoconductive response stability of the [Ru(L1)(L2)(NCS)$_2$] complex based photodiode was investigated by transient measurements under a fixed voltage to understand the photoconduction mechanism of device. Fig. 8 a) and b) reveal the transient photocurrent curves of the dye sensitized solar cell-based photodiode for rise time (t_R) and fall time (t_F) under solar light power from 20 to 100 mW/cm^2 at the fixed voltage of -3 V, respectively. The value of t_F, t_R and the band width of dye sensitized solar cell-based photodiode was defined as 0.48, 0.65 s and 0.54 Hz, respectively. As seen in Fig. 8, when the device is under photo illumination, the photocurrent suddenly increases and reaches to almost stable level; in the off state, it rapidly goes through its initial level. This indicates the photodiode behavior of the studied device. The increment in the photocurrent under photo illumination is due to the exited carriers by incident photon energy, and its decrement in turning off state is related to trapping the photogenerated carriers in deep levels [18–22]. This obtained results support the photosensitive property of the prepared dye sensitized solar cell-based photodiode; and it is possible to use in optoelectronic device fabrication such as a photodiode or photosensor.

The photoresponse ratio (R_{ph}) is defined by dividing the value of photocurrent by the dark current (I_{on}/I_{off}) for the photodiode. The value of R_{ph} was calculated and listed in Table 2 under the illumination power from 20 to 100 mW/cm^2 at different voltages. From the table, this value increases with the increasing in solar power at all voltage values; it reaches the maximum value of 200.69 under 100 mW/cm^2 at -1 V. The device gains the importance advantage with this higher photoresponse value for the photodiode application, when compared to that of literature value [14].

In order to satisfy noteworthy information about the behavior of photogenerated charges and their density as a function of time,

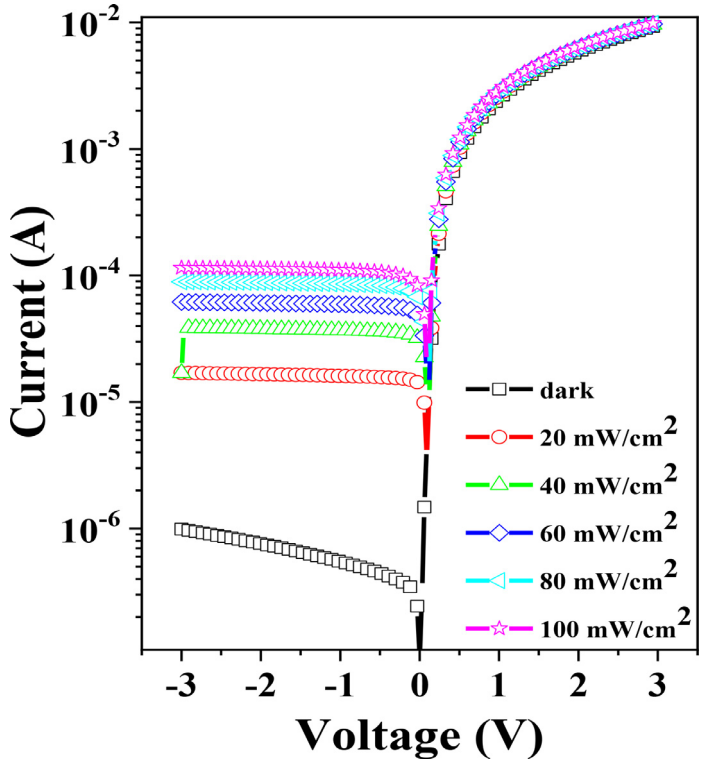

Fig. 5. The *I-V* plots of the photodiode under dark and various illumination intensities.

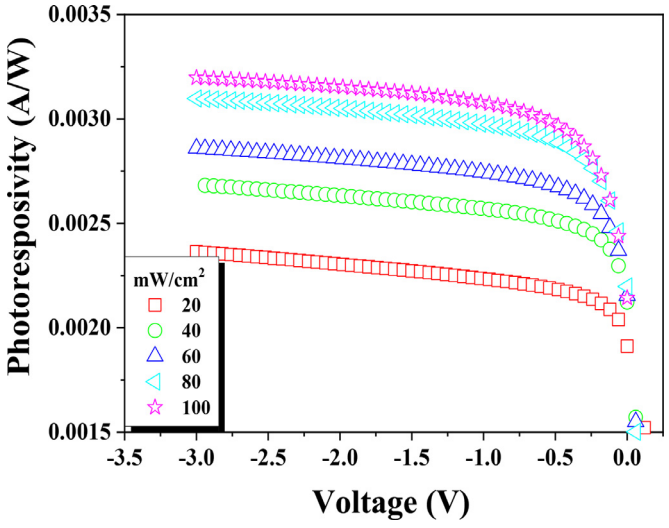

Fig. 6. The photoresponsivity-voltage plots of the photodiode at reverse biasing under various illumination intensities.

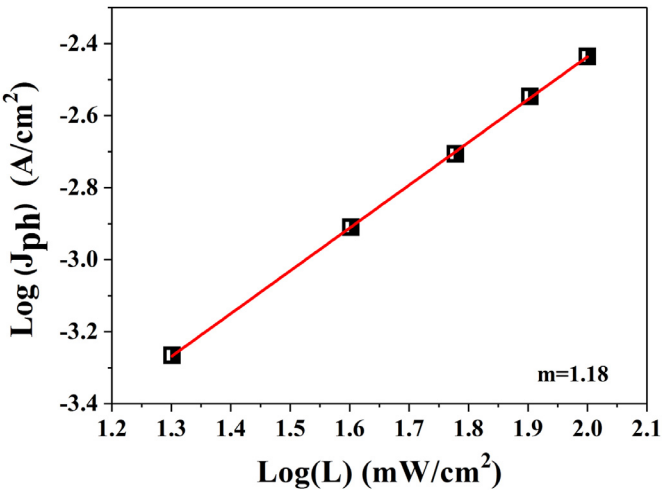

Fig. 7. The Log(J_{ph})- Log(L) curves of photodiode at -3 V.

the transient experiments were performed for the fabricated dye synthesized solar cell-based photodiode. Fig. 9 (a) and (b) show the transient photocapacitance and photoconductance characteristic of studied photodiode for various solar intensities at 10 kHz, respectively. It is seen from these figures that the sudden increase in photocapacitance up to certain value in state of solar power on was observed from Fig 9(a); and the rapid decrement up to its initial value is seen in the same when the power is switching off. This behavior can be associated with that the density of carries generated by photon varies between off/on states. The photoconductance has similar behavior in turning on and off states seen in Fig. 9 (b). Tataroglu et. al [3] presented the similar results for the Ru complex based photodiode [3]. Thus, these obtained results for dye sensitized solar cell-based photodiode declare that the studied device based on [Ru(L1)(L2)$(NCS)_2$] complex has the photocapacitive behavior.

3.3. Capacitance/conductance-voltage characteristics of the photodiode

For further analyzing of the capacitance profile of the photodiode, the *C-V* and *G-V* measurements were applied at different frequencies, depicted in Fig. 10 (a) and (b), respectively. Its capacitance remarkably changes with the applied voltage and the frequency, seen in Fig 10(a). Its dependency on frequency and voltage was characterized by a peak in the forward biasing (Fig 10a).

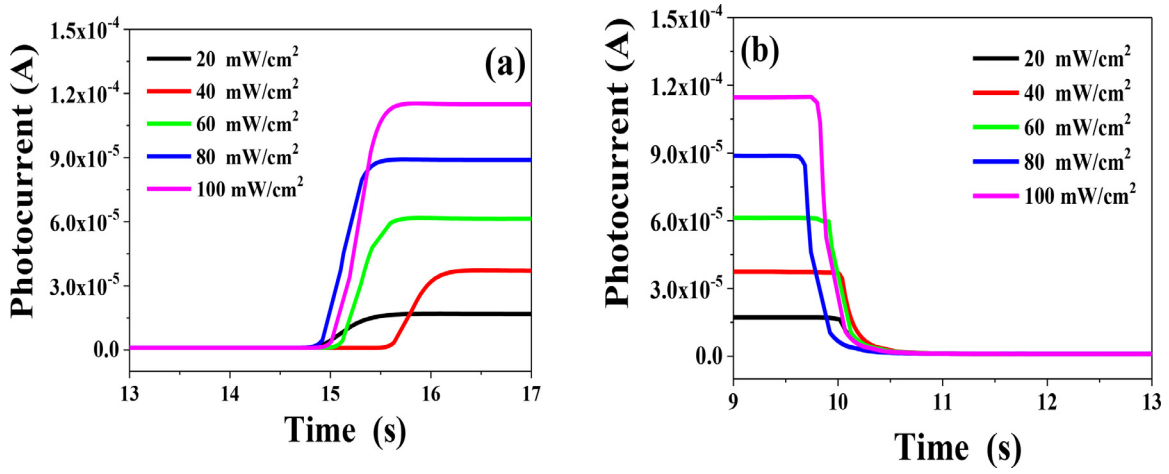

Fig. 8. The transient photocurrent a) t_R and b) t_F characteristic of the photodiode at -3 V.

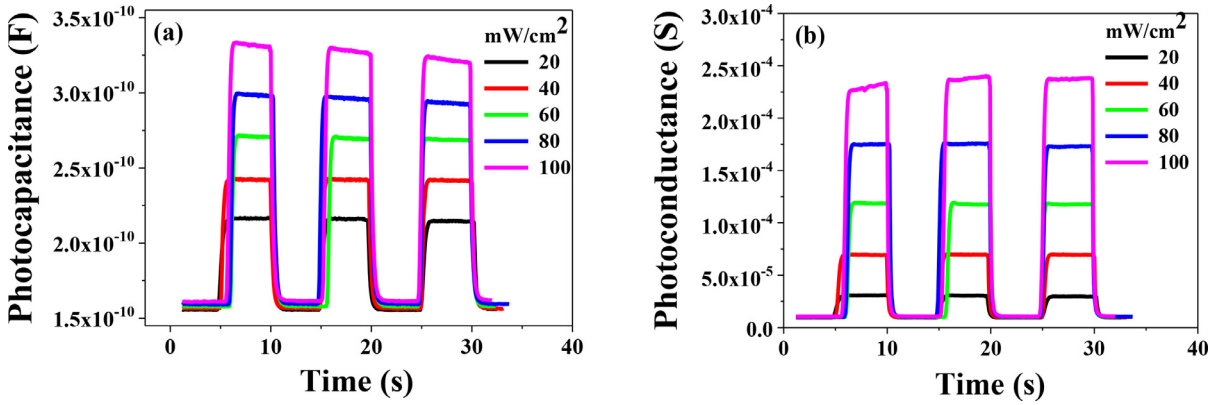

Fig. 9. The transient (a) Photocapacitance and (b) Photoconductance characteristics of the photodiode at -10 kHz.

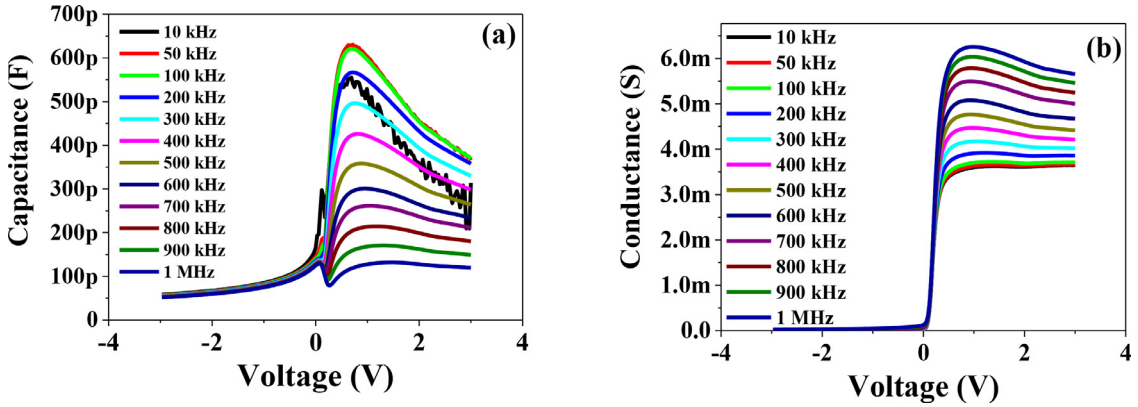

Fig. 10. The plots of (a) *C-V* and (b) *G-V* of photodiode under various frequencies.

The value of the capacitance peak increases with the decreasing in the frequency, related to behavior of the interface states [23–26]. Moreover, the value of G is dependent on the oscillation frequency and the applied voltage especially in the forward biasing for studied device (Fig. 10(b)). The conductance value of studied device increases with the increasing the frequency, due to the presence of interface states charges [25,27]. From these figures that the *C-V* and *G-V* characteristics of the photodiode almost don't change in the reverse bias regime. Dere et al. have reported similar findings about the C/G-V characteristics for the B-doped GO based photodiode [16].

The effect of series resistance (R_s) on the measured capacitance (C_m) and conductance (G_m) can be eliminated by adjusting with the following as corrected capacitance (C_{adj}) and conductance (G_{adj}) [16]

$$C_{adj} = \frac{\left[G_m^2 + (\omega C_m)^2\right] C_m}{a^2 + (\omega C_m)^2} \tag{4}$$

$$G_{adj} = \frac{\left[G_m^2 + (\omega C_m)^2\right] a}{a^2 + (\omega C_m)^2} \tag{5}$$

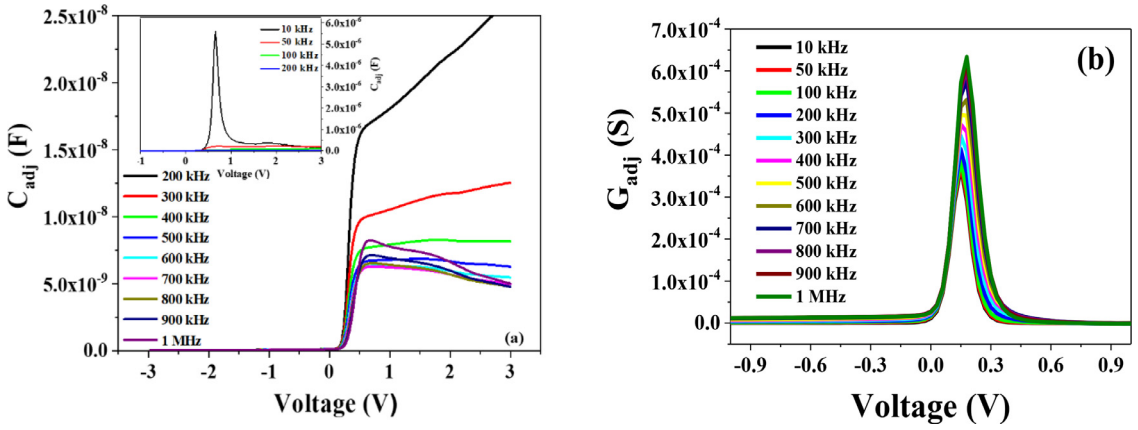

Fig. 11. The plots of (a) C_{adj}-V and (b) G_{adj}-V of photodiode under various frequencies.

herein, $a = G_m - [G_m^2+(\omega C_m)^2]R_s$. The plots of C_{adj} -V and G_{adj}-V for studied photodiode at different frequencies were automatically measured by FYTRONIX FY-7000 electronic devices characterization system. Fig. 11 a) and b) demonstrate the plots of C_{adj}-V and G_{adj}-V of photodiode under various frequencies, respectively.

The C_{adj}-V curves in the inset of Fig. 11 a) shows a sharp peak in the forward bias region just for the frequency of 10 kHz, which is related to the excess capacitance at this low frequency [23,28–30]. For further increasing in the frequency, the value of C_{adj} decreases, seen in the Fig. 11 a). A peak located at positive voltages in G_{adj}-V plot for all frequencies was seen in Fig. 11 b) due to the interface charges. Its position slightly shifts toward to the higher voltage, and its value enhances with increasing the frequency. Dere et al. [16] reported that this change in the C_{adj}-V and G_{adj}-V characteristics of the photodiode is caused by the effect of the series resistance.

4. Conclusions

The [Ru(L1)(L2)$(NCS)_2$] complex was synthesized and characterized by analytical and spectroscopic methods. The dye-sensitized solar cell-based photodiode exhibited both photoconductive and photovoltaic behavior. The photoresponse of the device was found to be about 200.69 under the illumination of 100 mW/cm^2 at -1 V. The phototransient measurements of the device show that the device can be optically switched with a stable behavior. The obtained optoelectronic parameters suggest that the prepared device using the [Ru(L1)(L2)(NCS)2] complex could be used in optoelectronic device for optical switching and controlling applications like photosensor/photodetector.

Author statement

There are not any conflict between authors.

Declaration of Competing Interest

The authors declare that they have no known competing financial interests or personal relationships that could have appeared to influence the work reported in this paper.

Acknowledgements

Authors would like to acknowledge the support of the King Khalid University for this research through a grant RCAMS/KKU under the (Research Center for Advanced Materials Science) at King Khalid University, Kingdom of Saudi Arabia.

References

[1] J.K. Nagle, J.S. Bernstein, R.C. Young, T.J. Meyer, Charge–transfer excited states as molecular photodiodes, Inorg. Chem. 20 (1981) 1760–1764.
[2] A.E. Ceniceros–Gomez, A. Ramos–Organillo, J. Hernandez–Dıaz, J. Nieto–Martınez, R. Contreras, S.E. Castillo–Blum, NMR study of the coordinating behavior of 2,6–bis(benzimidazol–2–yl)pyridine, Heteroat. Chem. 11 (2000) 392–398.
[3] A. Tataroglu, O. Dayan, N. Ozdemir, Z. Serbetci, A.A. Al–Ghamdie, A. Dere, F. El–Tantawy, F. Yakuphanoglu, Single crystal ruthenium (II) complex dye based photodiode, Dyes Pigm. 132 (2016) 64–71.
[4] A.O. Adeloye, P.A. Ajibade, Towards the development of functionalized polypyridine ligands for Ru(II) complexes as photosensitizers in dye–sensitized solar cells (DSSCs), Molecules 19 (2014) 12421–12460.
[5] P.A. Scattergood, U. Khushnood, A. Tariq, D.J. Cooke, C.R. Rice, P.I.P. Elliott, Photochemistry of $[Ru(pytz)(btz)^2]^{2+}$ and characterization of aκ^1–btz ligand–loss intermediate, Inorg. Chem. 55 (2016) 7787–7796.
[6] Y. Wang, W. Perez, G.Y. Zheng, D.P. Rillema, Syntheses and electrochemical, photophysical, and photochemical properties of ruthenium(II) 4,5–diazafluorenone complexes and their ketal derivatives, Inorg. Chem. 37 (1998) 2051–2059.
[7] E. Elgazzar, O. Dayan, Z. Serbetci, A. Dere, A.G. Al-Sehemi, A.A. Al-Ghamdi, F. El-Tantawy, W.A. Farooq, F. Yakuphanoglu, Heteroleptic neutral Ru(II) complexes based photodiodes, Physica B 516 (2017) 1–7.
[8] S. Yaşar, S. Çekirdek, N.Ertekin Binbay, A. Tombak, Y.S. Ocak, N. Arslan, A. Baysal, M. Aydemir, F. Durap, Electrical and photoelectrical characterization of organic-inorganic heterostructures based on Ru-N-heterocyclic carbene complexes, Optik 156 (2018) 514.
[9] S. Arounaguiri, B.G. Maiya, Electro-photo switch“ and "molecular light switch" devices based on ruthenium(II) complexes of modified dipyridophenazine ligands: modulation of the photochemical function through ligand design, Inorg. Chem. 38 (1999) 842–843.
[10] A. Tataroglu, R. Ocaya, A. Dere, O. Dayan, Z. Serbetci, A.G. Al-Sehemi, M. Soylu, A.A. Al-Ghamdi, F. Yakuphanoglu, Ruthenium(II) complex based photodiode for organic electronic applications, J. Electron. Mater. 47 (2018) 828–833.
[11] G. Tsukamoto, K. Yoshino, T. Kohno, H. Ohtaka, H. Kagaya, K. Ito, Synthesis and antiinflammatory activity of some 2– (substituted–pyridinyl) benzimidazoles, J. Med. Chem. 23 (1980) 734–738.
[12] C. Piguet, J.G. Bünzli, G. Bernardinelli, G. Hopfgartner, A.F. Williams, Self–assembly and photophysical properties of lanthanide dinuclear triple–helical complexes, J. Am. Chem.Soc. 115 (1993) 8197–8206.
[13] A. Tataroglu, F. Özen, K. Koran, A. Dere, A.O. Görgülü, N. Al-Senay A.A. Al-Ghamdi, W.A. Farooq, F. Yakuphanoglu, Structural, electrical and photoresponse properties of Si-based diode with organic interfacial layer containing novel cyclotriphosphazene compound, Silicon 10 (2018) 683–691.
[14] V. Ganesh, M. Aslam Manthrammel, Mohd. Shkir, I.S. Yahia, H.Y. Zahran, F. Yakuphanoglu, S. Al Faify, Organic semiconductor photodiode based on indigo carmine/n-Si for optoelectronic applications, Appl. Phys. A (2018), doi:10.1007/s00339-018-1832-x.
[15] A. Gencer Imer, O. Karaduman, F. Yakuphanoglu, Controlling of the photosensing properties of Al/DMY/p-Si heterojunctions by the interface layer thickness, Synth. Met. 221 (2016) 114.
[16] A. Dere, B. Coskun, A. Tataroğlu, A.G. Al-Sehemi, A.A. Al-Ghamdi, H.M.A. Alateeq, R. Qindeel, W.A. Farooq, F. Yakuphanoglu, Boron doped graphene based linear dynamic range photodiode, Physica B 545 (2018) 86.
[17] A.G. Imer, R.H.B. Syan, M. Gülcan, Y.S. Ocak, A. Tombak, The novel pyridine based symmetrical Schiff base ligand and its transition metal complexes: synthesis, spectral definitions and application in dye sensitized solar cells (DSSCs), J. Mater. Sci. Mater. Electron. 29 (2) (2018) 898.

[18] A. Tataroğlu, A.G. Al-Sehemi, M. Özdemir, R. Özdemir, H. Usta, A.A. Al-Ghamdi, W.A. Farooq, F. Yakuphanoglu, Frequency and electric field controllable photodevice: FYTRONIX device, Physica B 519 (2017) 53.
[19] A. Dere, A. Tataroğlu, Abdullah G. Al-Sehemi, Ahmed A. Al-Ghamdi, F. Farid El-Tantawy, W.A. Farooq, F. Yakuphanoglu, A functional material based photodiode for solar tracking systems, Physica B 520 (2017) 76.
[20] C.-Y. Tsay, W.-T. Hsu, Comparative studies on ultraviolet-light-derived photoresponse properties of ZnO, AZO, and GZO transparent semiconductor, Thin Films Mater. 10 (2017) 1379.
[21] A.G. Imer, A. Dere, A.G Al-Sehemi, O. Dayan, Z Serbetci, A.A. Al-Ghamdi, F. Yakuphanoglu, Photosensing properties of ruthenium (II) complex-based photodiode, Appl. Phys. A 125 (3) (2019) 1–10.
[22] W. Khan, S.-Dong Kim, Ultra-violet photo-response characteristics of p-Si/i-SiO2/n-ZnO heterojunctions based on hydrothermal ZnO nanorods, Mater. Sci. Semicond. Process. 66 (2017) 232.
[23] A. Gencer Imer, A. Tombak, A. Korkut, Electrical and photoelectrical characteristic investigation of a new generation photodiode based on bromothymol blue dye, J. Phys. Con. Series 707 (2016) 012012.
[24] A Tombak, A.G Imer, R.H.B Syan, M Gülcan, S Gümüş, Y.S. Ocak, Synthesis, characterization, DFT studies, and photodiode application of azo-azomethine-based ligand and its transition-metal complexes, J. Electron. Mater. 47 (12) (2018) 7240.
[25] I.S. Yahia, A.M. Shakra, M. Fadel, H.S. Hafez, M.M. Micheal, F. Yakuphanoglu, Photovoltaic response of dye-sensitized solar cell using 2′, 7′-dichlorofluorescein as an organic dye, Mater. Sci. Semicon. Proc. 28 (2014) 77.
[26] A. Ugur, A. Gencer Imer, Y.S. Ocak, Electrical and photoelectrical characterization of an organic–inorganic heterojunction based on quinoline yellow dye, Mater. Sci. Semicon. Proc. 39 (2015) 569.
[27] D.-T. Phan, R.K. Gupta, G.-S. Chung, A.A. Al-Ghamdi, O. A Al-Hartomy, F. El-Tantawy, F. Yakuphnaoglu, "Photodiodes based on graphene oxide–silicon junctions"Sol. Energy86 (10), 2961
[28] O. Dayan, A.G. Imer, A.G Al-Sehemi, N Özdemir, A Dere, Z Şerbetçi, A.A. Al-Ghamdi, F. Yakuphnaoglu, Photoresponsivity and photodetectivity properties of copper complex-based photodiode, J. Mol. Struct. 1200 (2020) 127062.
[29] A.G. Imer, A. Korkut, W.A. Farooq, A Dere, M Atif, A Hanif, A Karabulut, Interface controlling study of silicon based Schottky diode by organic layer, J. Mater. Sci. Mater. Electron. 30 (21) (2019) 19239.
[30] AG Imer, E Kaya, A Dere, AG Al-Sehemi, AA Al-Ghamdi, A Karabulut, Illumination impact on the electrical characteristics of Au/sunset yellow/n-Si/Au hybrid Schottky diode, J. Mater. Sci. Mater. Electron. 31 (17) (2020) 14665–14673.